processes

MDPI

Article

Experimental and Numerical Research on Swirl Flow in Straight Conical Diffuser

Dejan Ilić [1,*], Jelena Svorcan [2], Đorđe Čantrak [1] and Novica Janković [1]

[1] University of Belgrade, Faculty of Mechanical Engineering, Department of Hydraulic Machinery and Energy Systems, 11000 Belgrade, Serbia; djcantrak@mas.bg.ac.rs (Đ.Č.); njankovic@mas.bg.ac.rs (N.J.)
[2] University of Belgrade, Faculty of Mechanical Engineering, Department of Aerospace Engineering, 11000 Belgrade, Serbia; jsvorcan@mas.bg.ac.rs
* Correspondence: dilic@mas.bg.ac.rs

Abstract: The main objective of the current study is a detailed (both numerical and experimental) investigation of the highly unsteady and complex swirl flow in a straight conical diffuser (with a total divergence angle of 8.6°) generated by an axial fan impeller. Pressure, and axial and tangential velocity profiles along several cross-sections were measured by original classical probes in two different flow regimes at the inlet: the modified solid body type of moderate swirl and the solid body type of strong swirl and reverse flow; they were additionally confirmed/validated by laser Doppler anemometry measurements. Computational studies of spatial, unsteady, viscous, compressible flows were performed in ANSYS Fluent by large eddy simulation. The fan was neglected, and its effect was replaced by the pressure and velocity profiles assigned along the inlet and outlet boundaries. The two sets of data obtained were compared, and several conclusions were drawn. In general, the relative errors of the pressure profiles (2–5%) were lower than the observed discrepancies in the axial velocity profiles (5–40% for the first and 15–50% for the second flow regime, respectively). The employed reduced numerical model can be considered acceptable since it provides insights into the complexity of the investigated swirl flow.

Keywords: experiment; CFD; diffuser; turbulence; swirl; axial fan

check for updates

Academic Editor: Farhad Ein-Mozaffari

Received: 3 December 2024
Revised: 28 December 2024
Accepted: 3 January 2025
Published: 10 January 2025

Citation: Ilić, D.; Svorcan, J.; Čantrak, Đ.; Janković, N. Experimental and Numerical Research on Swirl Flow in Straight Conical Diffuser. *Processes* **2025**, *13*, 182. https://doi.org/10.3390/pr13010182

Copyright: © 2025 by the authors. Licensee MDPI, Basel, Switzerland. This article is an open access article distributed under the terms and conditions of the Creative Commons Attribution (CC BY) license (https://creativecommons.org/licenses/by/4.0/).

1. Introduction

The flow at the diffuser intake after an axial pump or axial fan impellers or in draft tubes after bulb turbines is an example of turbulent swirl flow that arises at turbomachines' exit. The draft tube of a bulb turbine is identical to a straight conical diffuser. The papers [1] provide an overview of the experimental research on turbulent flow in straight conical diffusers.

Investigations on swirl flow in draft tubes (conical diffusers) are aimed to improve hydraulic turbomachines' power parameters. The turbine runner induces swirl flow, which persists until the draft tube outlet, in a large region of turbine operation. Greater losses in the draft tube occur under operating conditions where the runner blades are more closed and where a significant swirl exists.

In general, the swirl flow in a diffuser is a highly challenging problem/flow case, both numerically and experimentally. Challenges stem from several reasons: complex fan geometry and computational domain, definition of adequate boundary conditions, non-isotropic turbulence (which cannot be adequately represented by the standard, usually employed unsteady Reynolds-averaged Navier–Stokes equation ((U)RANS) models), necessity to use fine computational meshes (detailed study in [2]), high unsteadiness and necessity to

use small time steps and perform long and computationally costly simulations, difficulties in reaching concrete conclusions (large-scale data processing and analysis), etc. Also, the value of the Coriolis coefficient at the diffuser's exit has a significant influence on accurate diffuser flow prediction using computational fluid dynamics (CFD) calculations.

Organic vapor flows within turbomachinery (the geometry comprised an elbow at the system inlet, a volute with a rotating impeller and a diffuser at the system outlet) were studied in [3]. Unstructured mesh and commercial CFD software ANSYS CFX 18.1 based on the finite volume method were employed, while RANS equations were closed by the k-ω shear stress transport (SST) turbulence model. This relatively standard numerical set-up provided numerical results that corresponded to the available experimental data with 15–20% accuracy.

Two examples of partial scale resolving methods, i.e., scale-adaptive simulation–(based on) shear stress transport (SAS-SST) and delayed detached eddy simulation (DDES) turbulence models, applied in the study of centrifugal fans and pumps are provided in [4,5]. The dynamic instability of swirl flow in a cyclone was investigated by measuring tangential velocity with hot-wire anemometry (HWA) and numerical simulations using large eddy simulation (LES) in the paper [6]. Based on the RANS approach, the study used unsteady numerical simulations of incompressible flow in a two-dimensional diffuser with a wide angle of 28° [7].

In the past two decades, the numerical research on swirl flow in conical diffusers has mostly focused on the flow in the draft tube of turbines. An unsteady solver was employed for the numerical simulation of flow when a free runner is installed in the draft tube cone (downstream of the main hydraulic runner turbine) based on the Generalized k-ω (GEKO) model in the paper [8]. The velocity componnts from the exit section of the swirl generator, obtained from experimental measurements, were imposed on the inlet boundary [8].

The RNG k-ε model and Spalart–Allmaras turbulence model (DDES-SA) applied for a conical diffuser (total angle of 17°) similar to the draft tube cone of a Francis turbine are discussed in [9]. The experimental (laser Doppler velocimetry (LDV)) and numerical (SST k-ω model) investigation of the draft tube after a Francis turbine was performed in [10].

Experimental (LDV) investigations of swirl flow in a hydraulic turbine discharge cone for 96 operating regimes "show that the large on-axis recirculation region, the precessing vortex rope, and the high level of velocity fluctuations occur at the shifting towards non-optimal regimes" [11].

The results of a hybrid RANS-LES and standard RANS simulation of Kaplan turbines were presented and compared to each other as well as measurements in the paper [12]. They have concluded the following, as the great challenge for researchers: "Currently, the most crucial flow features and primary influencing factors for precise simulations of Kaplan turbines, such as the turbulence model and time-step size, remain unclear" [12].

The numerical investigation of swirl flow in a straight conical diffuser (with a total divergence angle of 8.6°), as well as the comparison of the obtained results with the experimental investigations, is presented in this study. Similar experimental and numerical studies are relatively scarce, precisely due to the complexity of the investigated flow, and are usually validated through comparison with experimental data.

The peculiarity and novelty of the current study lie in the fact that the computational domain and grid are simplified as much as possible by neglecting the fan geometry. Instead, velocity and pressure profiles previously obtained through highly precise and accurate measurements and defined along the outer boundaries are used to compensate for this model reduction. Furthermore, a novel and computationally complex turbulence model is used for the closure of the flow equations and for capturing some of the flow phenomena typical of swirl flows.

In addition to the above, in this paper, the pressure profiles along the diffuser, measured by original classical probes, are presented, and they are compared with the ones obtained by numerical simulations. In most of the available papers in the literature, the pressure was measured only at the diffuser wall, not in the cross-section.

2. Experimental Research

The experimental test rig is shown in Figure 1 and described in detail in [13]. The straight steel conical diffuser (4) positioned in the chamber (5) comes after the axial fan impeller (2), with the rotational speed-controlled motor (1) and profiled inlet nozzle (3), which creates the swirl flow field. The test rig was equipped with a honeycomb (6), a flow meter (nozzle) (7), a pipe (8), a booster fan (9) and a flow regulator (10). The diffuser inlet diameter was D_0 = 0.4 m and the length was L = 1.79 m. By changing the fan impeller's rotation number, impeller blade angle, booster fan impeller's rotation number and flow regulator position, various regimes were created.

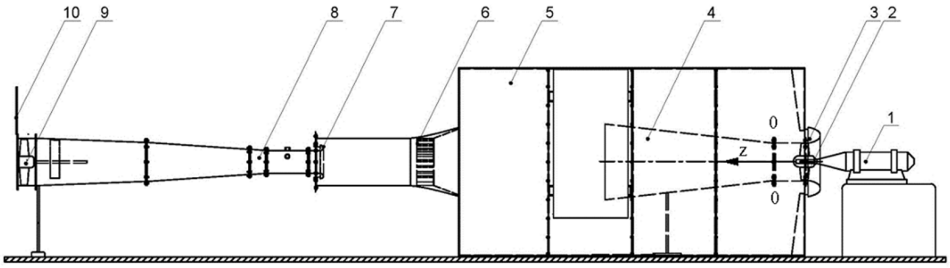


Figure 1. Test rig for experimental investigation [13].

The axial fan impeller, model AP 400 (Minel, Beograd, Serbia), had an outer diameter of 0.397 m and seven blades. The ratio of the hub and outer diameter, i.e., the non-dimensional radius, was ν = 0.434. Blades were adjusted at the angle of 40° for regime A (Table 1) and 29° for regime C (Table 1) at the outer diameter. The fan rotation speeds were n = 1400 min^{-1} for regime A and n = 1000 min^{-1} for regime C.

Table 1. Measuring series.

Series	Ω_0	S_0	$Re_0 \cdot 10^{-5}$	Type of Swirl Inflow Profiles
A	0.74	0.61	2.59	Modified solid body (moderate swirl)
C	0.12	1.46	0.53	Solid body (reverse flow and strong swirl)

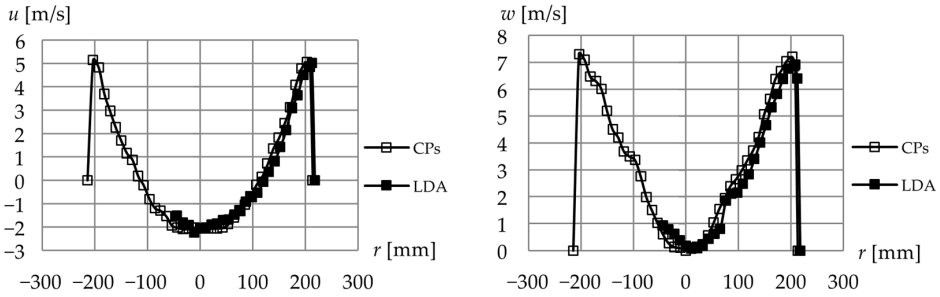
Originally, experimental measurements were performed to determine the energy characteristics and losses in the diffuser. For this reason, it was necessary to measure pressure profiles, as well as flow velocity profiles. The use of classical probes was justified by the fact that other measuring probes only measure flow velocity and not pressure.

Measurements of the swirl flow velocity components using laser Doppler anemometry (LDA) and a six-channel Conrad probe in the diffuser indicate that the radial velocity is significantly lower than the axial and circumferential velocities. On the basis of this, the assumption of two-dimensional flow was introduced.

Therefore, measurements were performed by using original home-made classical probes, combined Prandtl (Pitot-static) and angular probes. The velocity vector angle was determined by using an angle probe. The total pressure was measured by a combined Prandtl probe without a part (sleeve) attached, in which case it is a Pitot probe. The probe head's outer and inner diameters were 1.5 and 1 mm, respectively. Static pressure was measured at the same measurement position by using the combined Prandtl probe with the attached part (sleeve) with the two opposing 0.4 mm diameter holes drilled. The combined

Prandtl probe with the attached part was calibrated by using a standard Pitot probe (the calibration uncertainty was ±1.5%) and validated with the LDA system. The home-made classical probes are described in detail in [14].

The comparison of the velocity profile measurements obtained with LDA and classical probes (CPs) for regime C (Table 1) in Figure 2 shows a good level of data alignment and validates the usage of classical probes.



(**a**) (**b**)

Figure 2. Velocity distribution (LDA and CPs) in section 1 (z = 0.2 m) of diffuser for regime C (**a**) axial components u and (**b**) tangential (circumferential) components w of velocity.

LDA measurements were carried out by using a signal processor (BSA F30) and one-component LDA systems (Dantec Dynamics, Skovlunde, Denmark; laser power of 35 mW). A thermal fog machine (Antari Z3000II, Antari lighting and effects Ltd., Taoyuan City, Taiwan; liquid EFOG) was used to achieve seeding, and the axial fan AP 400 naturally pulled seeding into the test rig. For the LDA measurements, the cross-shaped slots were cut along the diffuser horizontal axis, and transparent foils were glued over these slots. Axial and circumferential velocities were successively measured in measurement section 1 (Figure 3) at the same measuring points. The LDA system operated in backscatter mode with a focal length of 285 mm, while the measurement volume dimensions were 0.1013 × 0.1008 × 1.013 mm^3. The velocity calibration uncertainty was 0.11% (coverage factor 2). The velocity resolution was better than 0.002% of the chosen velocity range. A traversing system was used for probe positioning with the accuracy of 0.43 mm.

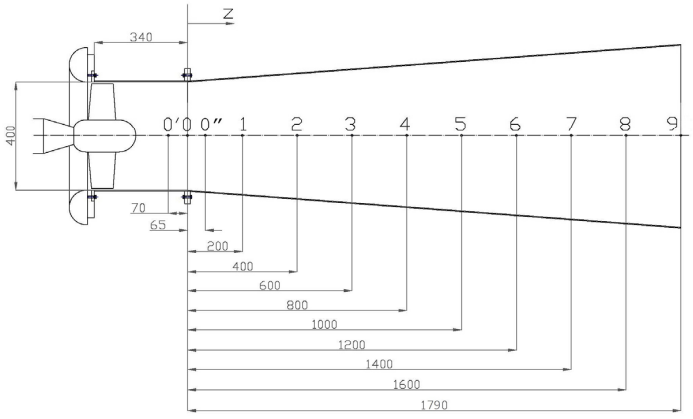


Figure 3. Measuring cross-section positions.

Velocity and pressure fields were measured with the classical probes at certain measuring cross-sections as given in Figure 3, with 0.05R (where D = 2R) steps between two measuring points (for example, 39 measuring points along diameter D_2). To measure static pressure on the wall, the diffuser had a small hole in the wall in each measuring cross-section.

The experimental data for two regimes, A and C, according to the regimes mentioned in the paper [13], are presented. Each measuring series, i.e., regime, is characterized by various parameters (Table 1): Ω—swirl flow parameter (or S—swirl number); Re—Reynolds number; and generated type of swirl inflow profiles (velocity, pressure and circulation). Subscript 0 refers to the inlet cross-section of the diffuser (Figure 3).

The swirl flow parameter [13] in the inlet cross-section is defined as

$$\Omega_0 = \frac{Q}{R_0 \Gamma_0}, \tag{1}$$

where the volume flow rate is calculated as

$$Q = 2\pi \int_0^{R_0} ru\mathrm{d}r, \tag{2}$$

and the average circulation is given as

$$\Gamma_0 = \frac{4\pi^2}{Q} \int_0^{R_0} r^2 w u dr. \tag{3}$$

The swirl number [13] is defined as

$$\mathrm{S}_0 = \frac{1}{2\beta_0 \Omega_0}, \tag{4}$$

where the Boussinesq number [13] is defined as

$$\beta_0 = \frac{2\pi\rho \int_0^{R_0} u^2 r dr}{\pi\rho u_m^2 R_0^2}. \tag{5}$$

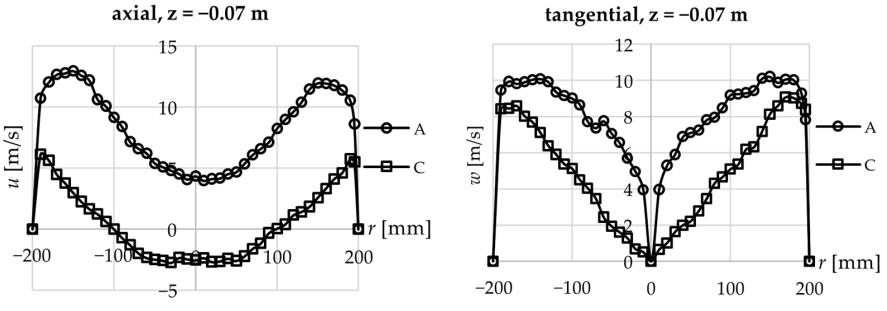
The average axial velocity is defined as

$$u_{m_0} = \frac{Q}{\pi R_0^2}. \tag{6}$$

Reynolds number:

$$\mathrm{Re}_0 = \frac{u_{m0} D_0}{\nu}. \tag{7}$$

The generated types of swirl inflow profiles in section 0′ (Figure 3; 70 mm upstream of the diffuser inlet, in a straight pipe after the fan impeller) are presented in Figure 4.



(**a**) (**b**)

Figure 4. Types of swirl inflow profiles for regimes A and C for (**a**) axial components u and (**b**) tangential (circumferential) components w of velocity.

3. CFD Calculations

The computational methodology is relatively straightforward and is described step by step. A numerical investigation was performed for regimes A and C.

3.1. Diffuser Geometry and Computational Domain

Two-dimensional axisymmetric simulations were initially performed, but since they were not able to adequately capture the complexity of the investigated swirl flow, we proceeded with full 3D analyses.

An initial sketch (closed contour defining the inlet radius of 0.2 m, axis of length 0.07 m (straight pipe) + 1.79 m (diffuser), outlet radius of 333.25 mm and outer wall) was revolved around the z-axis (see Figure 5 below), and inlet, outlet and wall surfaces were defined.

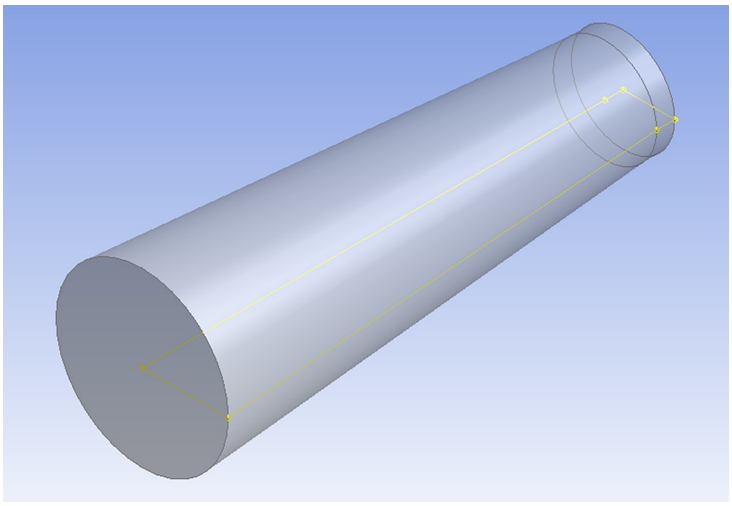


Figure 5. Computational domain.

3.2. Computational Meshes

Several meshes (differing in refinement level and number of cells, starting from 2.2 million control volumes (Mcvs) to 5 Mcvs and up 12 Mcvs, were generated and tested in the first flow regime. The resulting averaged velocity profiles were compared. Since all three inspected grids provided similar results, whereas computational complexity drastically increased on finer meshes, most of the simulations were performed on the coarsest mesh containing 2.2 Mcvs (illustrated in more detail in Figure 6).

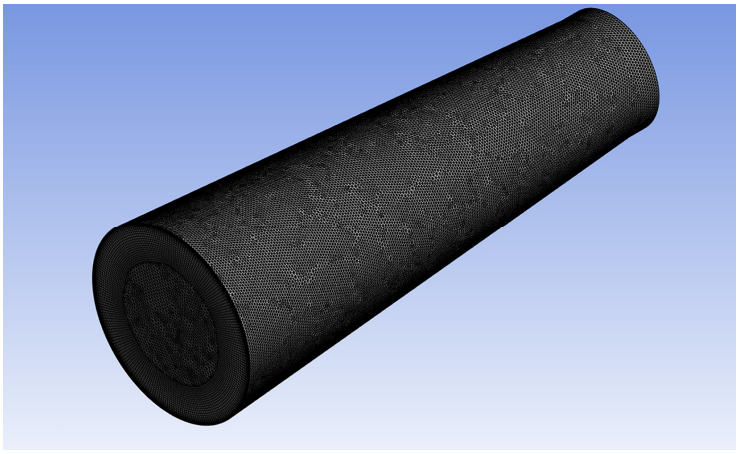


Figure 6. Computational mesh.

Overall, global cell size was defined (0.01 m for the coarsest mesh and lower, e.g., 0.007 m and 0.005 m for the medium and fine meshes, respectively), as well as the thin layers of prismatic cells stemming from the wall ($y1$ = 0.001 mm, N = 25 and q = 1.2, resulting in $y+$ around 20–30).

3.3. Computational Set-Up

All simulations were performed by using ANSYS Fluent, where the conservation equations for mass, momentum and energy governing the flow are solved by the finite volume method. Flow was considered three-dimensional (3D), unsteady, turbulent and compressible. Air was assumed to be an ideal gas with viscosity changing according to the Sutherland law. Turbulence was resolved by wall-modeled large eddy simulation (WMLES). This model is more recent but also more computationally expensive than the standardly employed RANS models and is capable of resolving a large portion of turbulent motion, which is the main reason why it was employed in this study.

In order to further simplify the simulations, the fan was not included, but the measured axial u and tangential (circumferential) w velocity profiles (illustrated in Figure 4), as well as the pressure p profiles, were defined along the inlet boundary. Since these flow variables depend on the radial coordinate, user-defined profiles (discrete arranged pairs of values) were created and used as boundary conditions. Similarly, the pressure profile was prescribed along the outlet surface (Table 2). All flow simulations were initialized from the steady state.

Table 2. Boundary conditions.

Surface	Boundary Conditions	Input
Inlets	u and w velocity profiles	u, w [m/s]
Outlets	Pressure profile	p [Pa]

A pressure-based coupled solver is employed. All numerical schemes are of the second order. The Courant number was limited to 10, while 10–20 iterations were performed in each time step of Δt = 0.001 s. Computations were performed until reaching quasi-convergence (convergence of mean values), which is usually achieved within several seconds.

4. Results and Discussion

Everything is highly sensitive to the time step and the number of sub-iterations and less so to the mesh and (partially scale resolving) turbulence model. During the computation, the velocity and pressure profiles along characteristic cross-sections were registered (Figure 3) for $z = -0.07$ m; 0.2 m; 0.6 m; 1.0 m; 1.2 m; 1.4 m; 1.79 m.

4.1. Velocity Profiles

The computed (full line) and measured (triangular markers) mean velocity profiles for regime A are illustrated in Figure 7.

The presence of circumferential velocity strongly influences the axial velocity profiles. The general trend seems captured, but there are also some discrepancies. A few flow visualizations are also presented in Figures 8–10. The figures show the complex structure of the non-uniform, turbulent swirl flow in the diffuser.

The velocity contours show strong vortex structures (Figure 8). The total velocity profile is strongly influenced by the presence of the circumferential velocity of almost the same intensity (Figure 9). The vortex core region could be observed and its dynamics investigated. It was followed by the numerous smaller vortical structures, which, by the Richardson law and Kolmogorov scale [15], related to the flow dissipation rate (Figure 10).

The computed (full line) and measured (triangular markers) mean velocity profiles for regime C are illustrated in Figure 11.

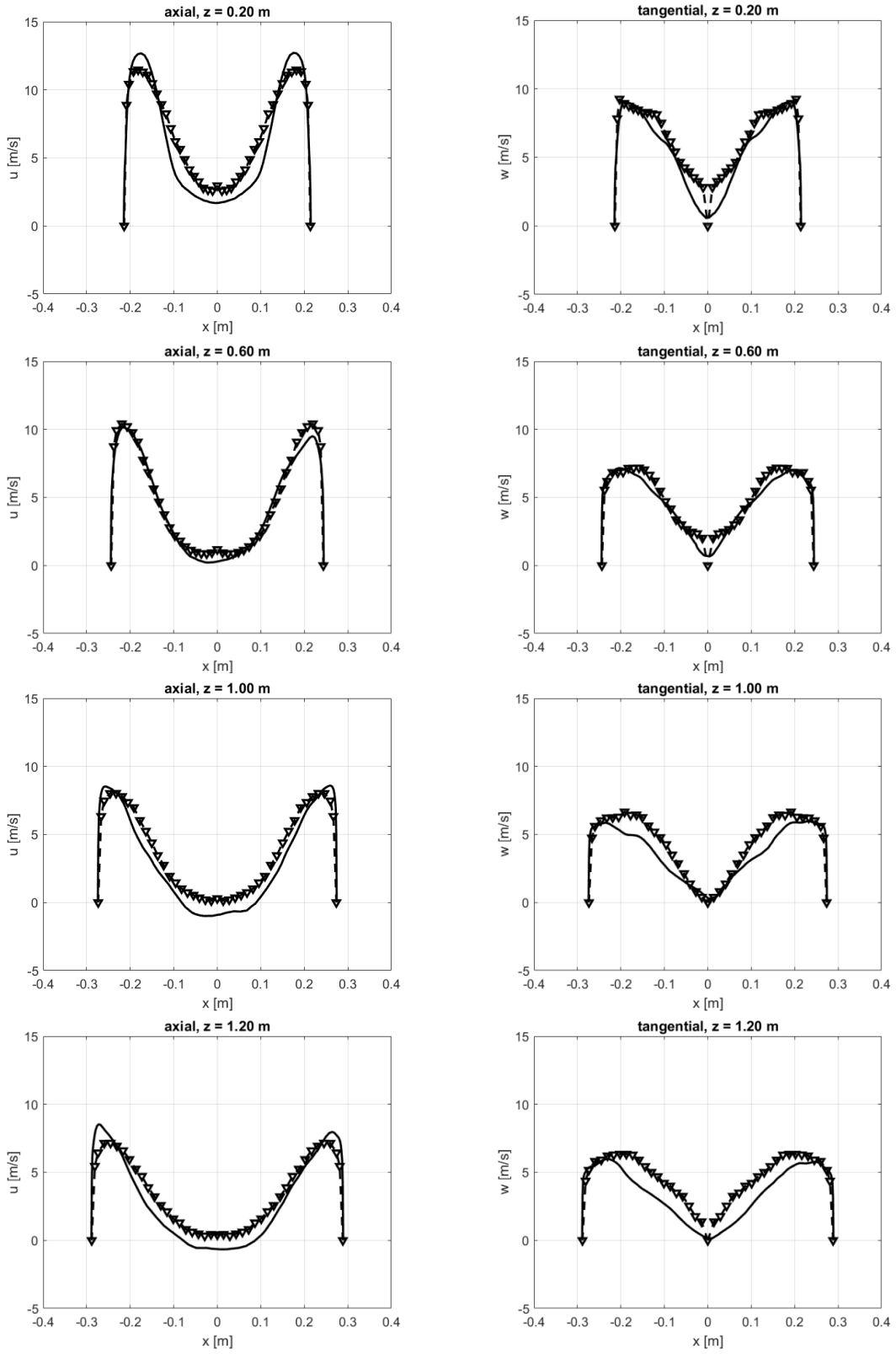


Figure 7. *Cont.*

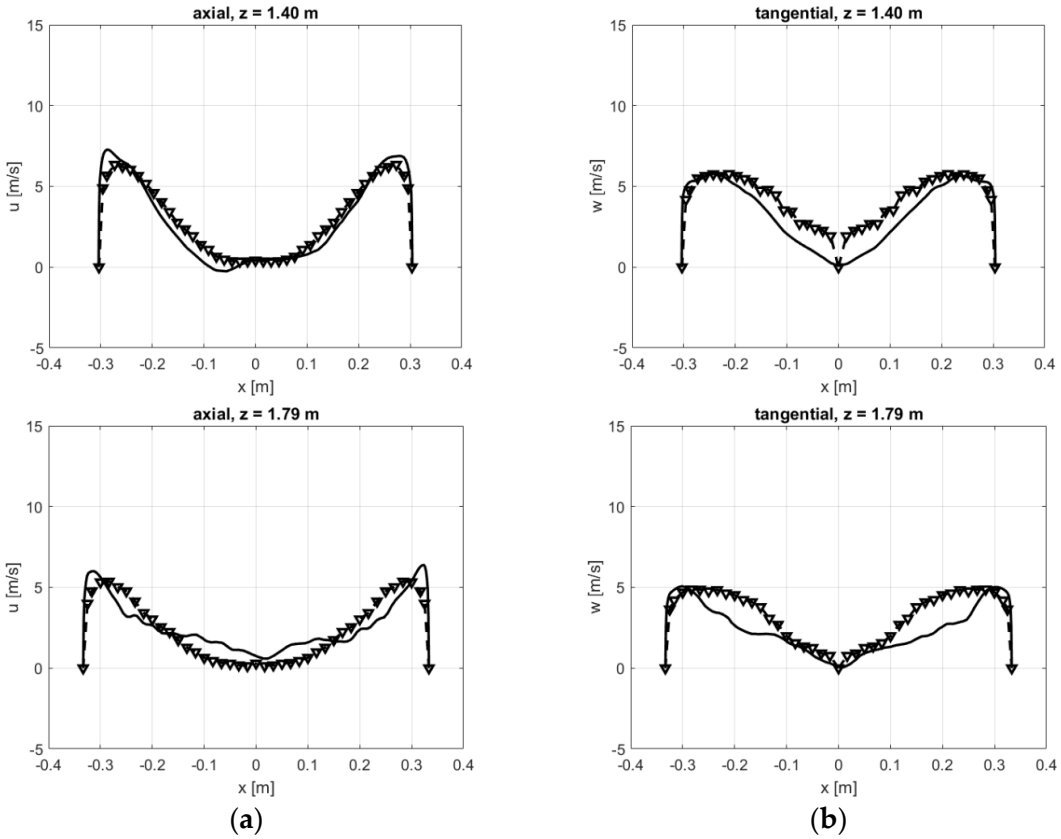


Figure 7. Regime A—velocity profiles: (**a**) axial components u of velocity along diffuser; (**b**) tangential (circumferential) components w of velocity along diffuser.

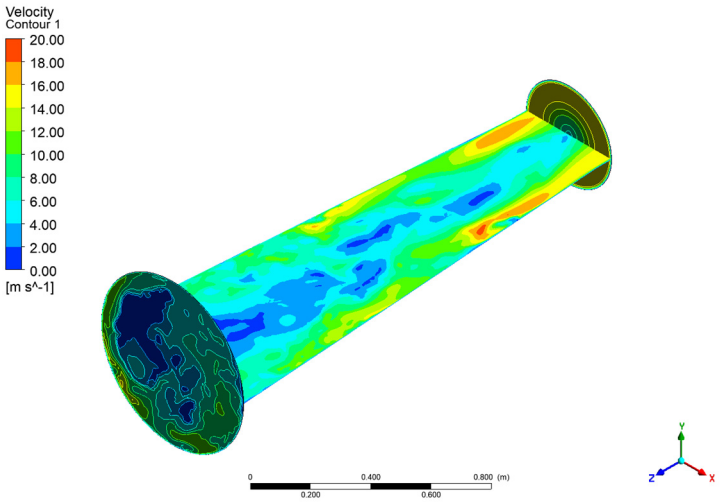


Figure 8. Regime A—computed instantaneous velocity contours.

It can be concluded that for regime A (with the inlet modified solid body type of moderate swirl), the computed axial velocity profiles better agreed with the measured profiles. For regime C (with the inlet solid body type of strong swirl and reverse flow), the computed axial velocity profiles in the section (z = 0.2 m) near the inlet section of the diffuser had some discrepancies from the measured axial velocity profiles. After that, along the diffuser, the computed axial velocity profiles agreed better with the measured velocity profiles. For regime A, in the diffuser core where $0 < r/R < 0.6$ and near the diffuser wall where $0.9 < r/R < 1$, the relative errors were the largest and amounted to 5–40%, while in the area where $0.6 < r/R < 0.9$, the relative errors were lowest and amounted to 5–15%,

depending on the measuring section. For regime C, in the diffuser core where $0 < r/R < 0.6$ and near the diffuser wall where $0.9 < r/R < 1$, the relative errors were also the largest and amounted to 15–50% or 80% for section 0′ (z = 0.2 m) in the diffuser core where $0 < r/R < 0.6$, while in the area where $0.6 < r/R < 0.9$, the relative errors were around 15%.

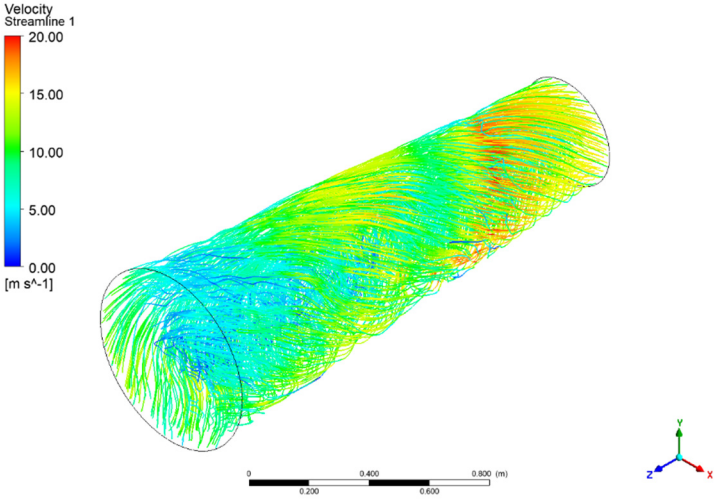


Figure 9. Regime A—computed instantaneous streamlines.

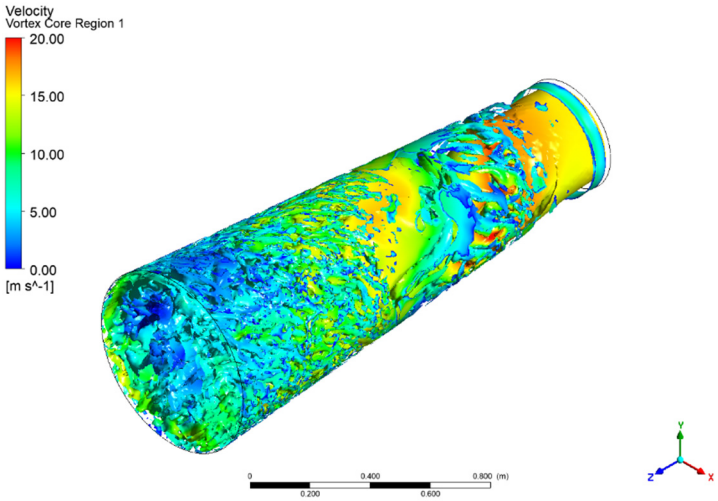


Figure 10. Regime A—computed instantaneous vortex core (vortical structures).

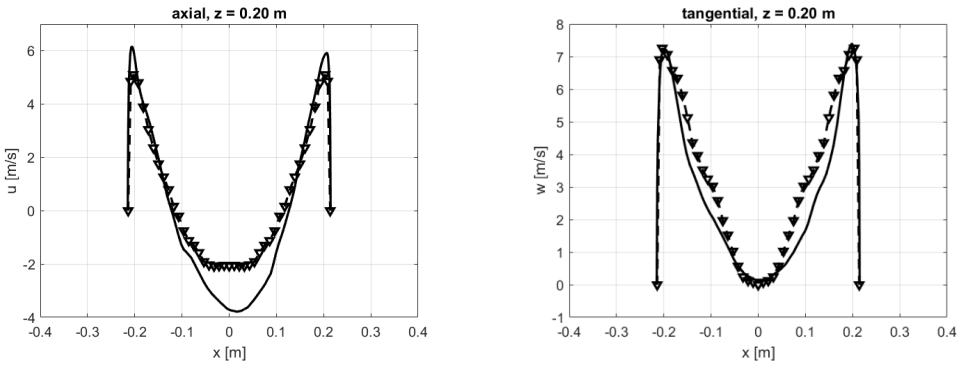


Figure 11. *Cont.*

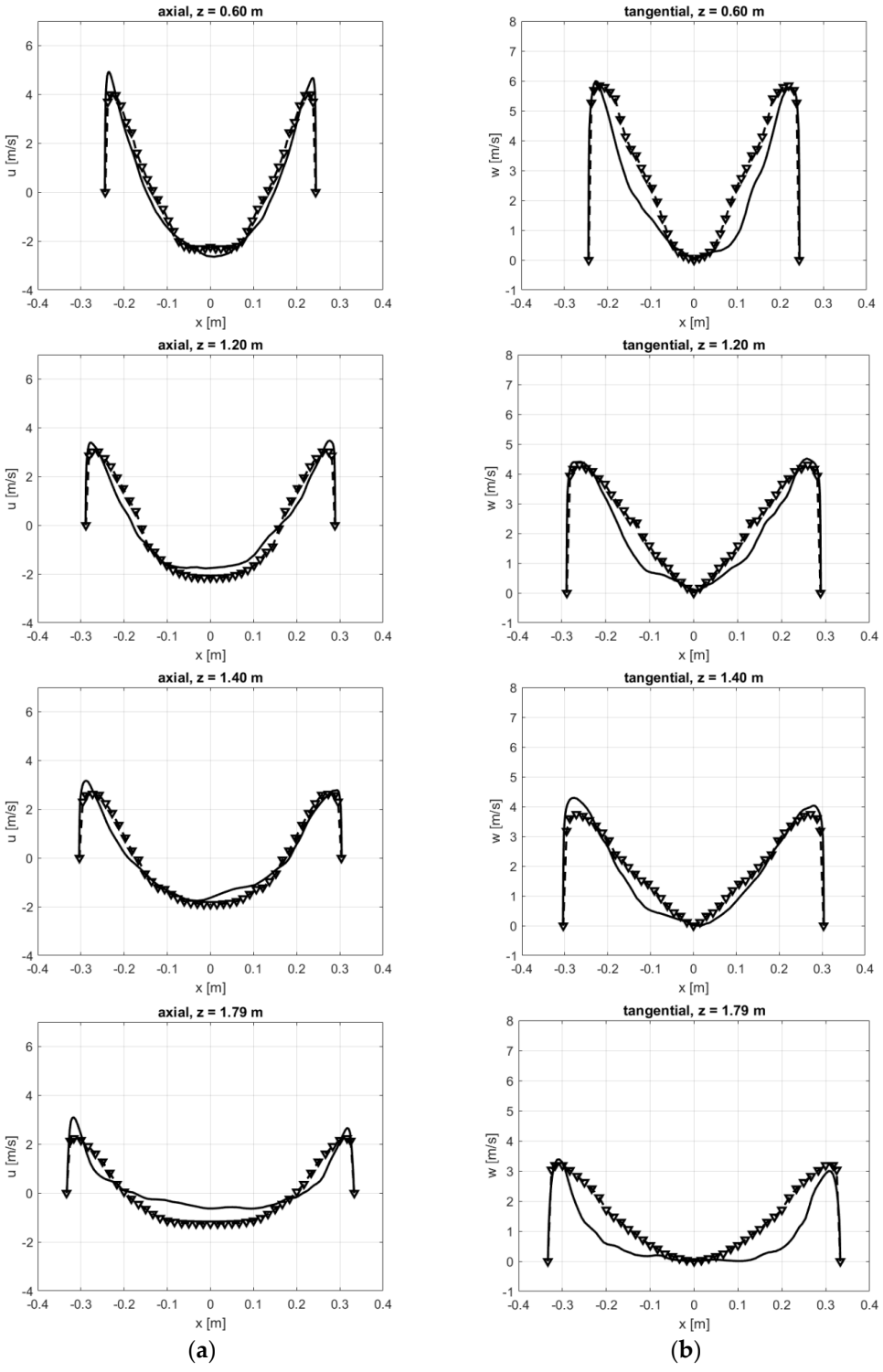


Figure 11. Regime C—velocity profiles: (**a**) axial components u of velocity along diffuser; (**b**) tangential (circumferential) components w of velocity along diffuser.

For both regimes, A and C, the tangential (circumferential) velocity profiles had some discrepancies from the measured profiles. The last profile of tangential (circumferential) velocity for both regimes was the most different, probably due to the imposed boundary conditions at the outlet (we neglected the chamber (5) in Figure 1). For both regimes A and C, in the diffuser core where $0 < r/R < 0.4$, the relative errors were the largest and amounted to 10–80%, and in the area where $0.4 < r/R < 0.7$, the relative errors amounted to 10–40%

depending on the measuring section, while in the area where $0.7 < r/R < 0.9$, the relative errors were up to 10%.

4.2. Pressure Profiles

The computed (full line) and measured (triangular markers) pressure profiles for regimes A and C are illustrated in Figure 12.

It can be concluded that for regimes A (especially) and C, the computed pressure profiles in the section (z = 0.2 m) near inlet section of the diffuser had some discrepancies from the measured pressure profiles. After that, along the diffuser, the computed pressure profiles agreed better with the measured pressure profiles. For regime A, for section 0′ (z = 0.2 m) in the diffuser core where $0 < r/R < 0.4$, the relative errors were the largest and amounted to 50–10%, and in area where $0.4 < r/R < 1$, the relative errors were around 7%, while for all other measurement sections in the entire cross-section where $0 < r/R < 1$, the relative error was less than 5%. For regime C, for section 0′ (z = 0.2 m) in the diffuser core where $0 < r/R < 0.4$, the relative errors amounted to 1.5–3%, and in the area where $0.4 < r/R < 1$, the relative errors were 3–7%, while for all other measurement sections in the entire cross-section where $0 < r/R < 1$, the relative error was less than 2%.

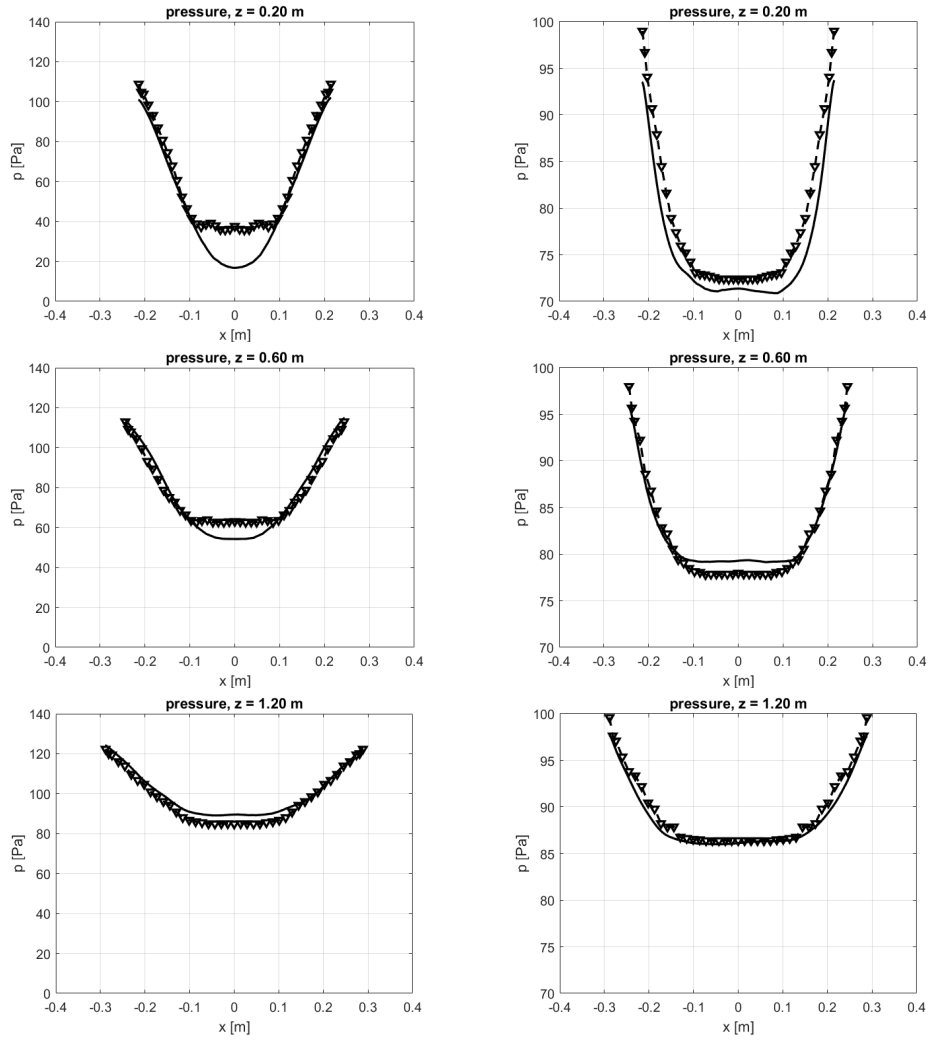


Figure 12. *Cont.*

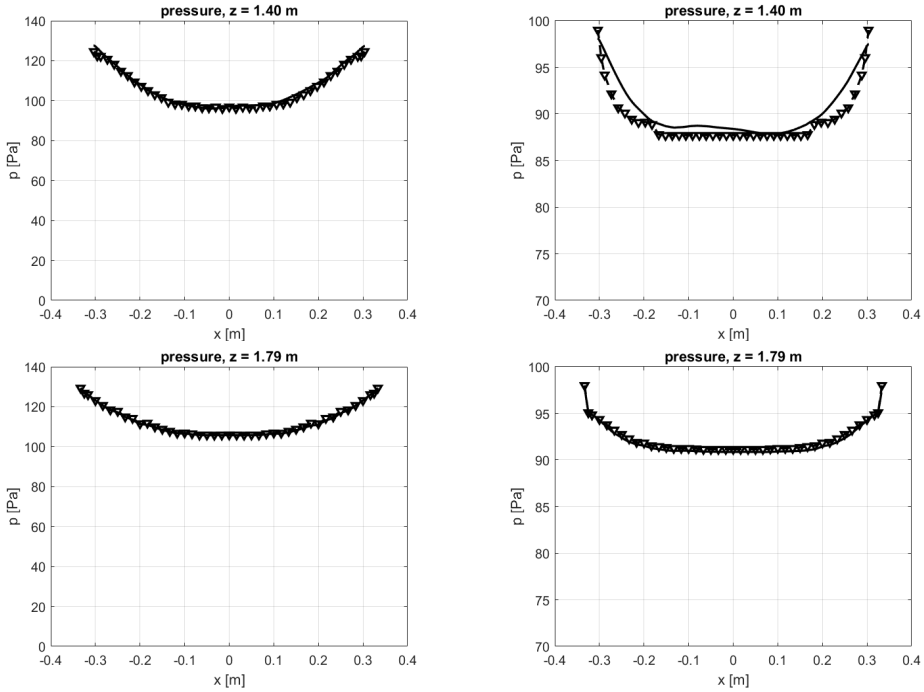


Figure 12. Pressure profiles along diffuser for (**a**) regime A and (**b**) regime C.

5. Conclusions

Comparative experimental and numerical investigations performed on a straight conical diffuser with a total divergence angle of 8.6° for two different regimes and swirl types are presented.

In general, it is very demanding to accurately measure velocity and pressure with classical probes and even more complex with LDA through the curved wall of the diffuser. The experimental results obtained by these two techniques were compared, and there was good overlapping. The measurements had a good sampling rate, as well as validation. The experimental results obtained in the inlet section of the diffuser after the swirl generator, which was an axial fan impeller, were carefully checked and thoroughly analyzed because they present the inlet data for numerical calculation.

Few numerical models were applied (both two- and three-dimensional, from standard RANS to partially scale resolving WMLES). The finally used numerical model provided good axial velocity profile prediction and agreement with the experimental results for an inlet moderate-strength modified solid body swirl (regime A). For regime C with the inlet solid body type of strong swirl and reverse flow, the overlap of the axial velocity profiles is acceptable if the initial diffuser cross-sections are excluded. Except for the initial diffuser cross-sections for regime A, the overlap of the pressure velocity profiles is also acceptable for both regimes (relative pressure errors are less than 5% for regime A and 2% for regime C). Based on the presented experimental and numerical data, it can be concluded that the relative errors were the largest (5–40% for regime A and 15–50% for regime C, for the axial velocity profiles) in the diffuser core and near the diffuser wall, which is a consequence of the complex flow field.

Due to the flow and geometry complexity, the authors consider this study a step towards a further better understanding of this complex flow phenomenon. Further numerical investigations could cover a wider computational domain, including more detailed geometry of the fan and the chamber in which the diffuser is located, the use of even finer computational meshes and the application of other turbulence models.

Author Contributions: Conceptualization and methodology, all authors; formal analysis, all authors; experimental investigation, D.I. and N.J.; numerical investigation, J.S.; writing, D.I., Đ.Č. and J.S. All authors have read and agreed to the published version of the manuscript.

Funding: This research was funded by the Ministry of Science, Technological Development and Innovation of the Republic of Serbia under the Agreement on financing the scientific research work of teaching staff at accredited higher education institutions in 2024, No. 451-03-65/2024-03/200105, dated 5 February 2024.

Data Availability Statement: The original contributions presented in this study are included in the article. Further inquiries can be directed to the corresponding author.

Acknowledgments: The results presented in this paper are the results of research supported by the Ministry of Science, Technological Development and Innovation of the Republic of Serbia under the Agreement on financing the scientific research work of teaching staff at accredited higher education institutions in 2024, No. 451-03-65/2024-03/200105, dated 5 February 2024.

Conflicts of Interest: The authors declare no conflict of interest.

References

1. Azad, R.S. Turbulent Flow in a Conical Diffuser: A Review. *Exp. Therm. Fluid Sci.* **1996**, *13*, 318–337. [CrossRef]
2. Seifollahi Moghadam, Z.; Guibault, F.; Garon, A. On the Evaluation of Mesh Resolution for Large-Eddy Simulation of Internal Flows Using Openfoam. *Fluids* **2021**, *6*, 24. [CrossRef]
3. Reinker, F.; Wagner, R.; Hasselmann, K.; aus der Wiesche, S.; Fritsche, M.; Epple, P.; Rußwurm, H.J. Testing, modeling and simulation of fans working with organic vapors. In Proceedings of the 13th European Conference on Turbomachinery Fluid Dynamics & Thermodynamics ETC13, Lausanne, Switzerland, 8–12 April 2019.
4. Pritz, B.; Probst, M.; Wiśniewski, P.; Dykas, S.; Majkut, M.; Smołka, K. Identification of unsteady effects in the flow through a centrifugal fan using CFD/CAA methods. *Arch. Thermodyn.* **2021**, *42*, 169–181. [CrossRef]
5. Du, L.; Zheng, F.; Gao, B.; Gad, M.; Li, D.; Zhang, N. Numerical Investigation of Rotor and Stator Matching Mode on the Complex Flow Field and Pressure Pulsation of a Vaned Centrifugal Pump. *Energies* **2024**, *17*, 2416. [CrossRef]
6. Sun, L.; Li, J.; Xie, M.; Man, M.; Zhao, J.; Song, J. A Numerical Simulation Study of the Dynamic Instability of Gas Swirling Flows in Cyclones. *Processes* **2024**, *12*, 2002. [CrossRef]
7. Meng, X.; Zuo, Z.; Nishi, M.; Liu, S. A Numerical Study on the Flow Mechanism of Performance Improvement of a Wide-Angle Diffuser by Inserting a Short Splitter Vane. *Processes* **2020**, *8*, 143. [CrossRef]
8. Bosioc, A.I.; Szakal, R.-A.; Stuparu, A.; Susan-Resiga, R. Numerical Analysis of the Flow by Using a Free Runner Downstream the Francis Turbine. *Int. J. Turbomach. Propuls. Power* **2023**, *8*, 14. [CrossRef]
9. Javadi, A.; Bosioc, A.; Nilsson, H.; Muntean, S.; Susan-Resiga, R. Experimental and Numerical Investigation of the Precessing Helical Vortex in a Conical Diffuser, With Rotor–Stator Interaction. ASME. *J. Fluids Eng.* **2016**, *138*, 081106. [CrossRef]
10. Ji, L.; Xu, L.; Peng, Y.; Zhao, X.; Li, Z.; Tang, W.; Liu, D.; Liu, X. Experimental and Numerical Simulation Study on the Flow Characteristics of the Draft Tube in Francis Turbine. *Machines* **2022**, *10*, 230. [CrossRef]
11. Skripkin, S.; Tsoy, M.; Kuibin, P.; Shtork, S. Swirling flow in a hydraulic turbine discharge cone at different speeds and discharge conditions. *Exp. Therm. Fluid Sci.* **2019**, *100*, 349–359. [CrossRef]
12. Joßberger, S.; Riedelbauch, S. Scale-Resolving Hybrid RANS-LES Simulation of a Model Kaplan Turbine on a 400-Million-Element Mesh. *Int. J. Turbomach. Propuls. Power* **2023**, *8*, 26. [CrossRef]
13. Ilić, D.; Benišek, M.; Čantrak, Đ. Experimental investigations of the turbulent swirl flow in straight conical diffusers with various angles. *Therm. Sci.* **2017**, *21* (Suppl. S3), 725–736. [CrossRef]
14. Benišek, M.H.; Lečić, M.R.; Ilić, D.B.; Čantrak, Đ.S. Aplication of New Classical Probes in Swirl Fluid Flow Measurements. *Exp. Tech.* **2010**, *34*, 74–81. [CrossRef]
15. Kolmogorov, A.N. A refinement of previous hypotheses concerning the local structure of turbulence in a viscous incompressible fluid at high Reynolds number. *J. Fluid Mech.* **1962**, *13*, 82–85. [CrossRef]

Disclaimer/Publisher's Note: The statements, opinions and data contained in all publications are solely those of the individual author(s) and contributor(s) and not of MDPI and/or the editor(s). MDPI and/or the editor(s) disclaim responsibility for any injury to people or property resulting from any ideas, methods, instructions or products referred to in the content.